IEEE Access
Multidisciplinary | Rapid Review | Open Access Journal

Received November 9, 2019, accepted November 25, 2019, date of publication November 28, 2019,
date of current version December 13, 2019.

*Digital Object Identifier 10.1109/ACCESS.2019.2956630*

# W Band Imaging System Using Linear Sparse Periodic Antenna Array and Compressive Sensing for Personnel Screening

**SHAOQING HU, (Student Member, IEEE), CHAO SHU, (Student Member, IEEE), YASIR ALFADHL, (Senior Member, IEEE), AND XIAODONG CHEN, (Fellow, IEEE)**
School of Electronic Engineering and Computer Science, Queen Mary University of London, London E1 4NS, U.K.
Corresponding authors: Chao Shu (c.shu@qmul.ac.uk) and Xiaodong Chen (xiaodong.chen@qmul.ac.uk)

**ABSTRACT** This paper presents our study on a W band imaging system consisting of a linear sparse periodic antenna array (SPA) with only 10 transmitting (Tx) and 10 receiving (Rx) elements in simulation and experiment for the purpose of personnel screening. We have devised a simplified and low cost experimental set-up using only 1 Tx and 1 Rx channels located on two scanning tracks separated by a distance to verify the proposed multi-static array imaging scheme. The simulation has taken account of the effects of track separation and measured antenna patterns. The simulation and experiment correlate quite well, indicating a resolution of about 7 mm at 1.3 m distance. Furthermore, based on the experimental data, we have investigated the compressive sensing (CS) image reconstruction as an approach for further reducing the sampling points in such a multi-static array imaging system. It is shown that using a discrete SPA-CS imaging algorithm, the images can be successfully reconstructed with the data as few as 30% of that used in the traditional holographic/synthetic aperture radar (SAR) imaging algorithm. Therefore, the CS image reconstruction is proved to be feasible for building a low-cost and fast millimeter wave imaging system.

**INDEX TERMS** Sparse periodic antenna array (SPA), holographic/synthetic aperture radar (SAR) imaging, compressive sensing (CS).

## I. INTRODUCTION

There are demands for millimeter wave (MMW) personnel screening systems for detecting concealed threats like handguns, knives and explosive devices in public areas, such as airports and train stations. Therefore, it requires the imaging system to have high resolution for correct identification and fast imaging rate for checking a large flow of people. In addition, the cost of the MMW imaging system should be low for a wide deployment.

In contrast to a passive imaging system that relies on temperature and/or emissivity contrast to form images at a fast rate [1]–[5], an active imaging system transmits MMW signals and collects the reflected signals from the target to construct high quality images by using various advanced imaging algorithms [6]–[13]. However, the current active imaging products in the commercial market still mainly work at lower millimeter wave band because of availability of the matured and low-cost electronic components [6]. For example, the Pro Vision in L3-Safe View licensed by the Pacific Northwest National Laboratory(PNNL) operates within the 24.25∼30 GHz band, incorporating two vertical linear antenna arrays with 384 antenna elements in each array [7]. In addition to the high cost due to using a large number of antenna elements and back-end channels, these active imaging systems also suffer poor resolution. Therefore, it is desirable to develop a W band or even higher band MMW imaging system for improved resolution. However, the imaging systems at these higher frequencies are mostly the prototypes in the lab, not commercial products due to high building cost. For example, it needs 1001 elements for a uniform array to scan a 1.5 m height at 100 GHz with an element/sampling spacing of half wavelength. Therefore, the sparse antenna array also known as the multiple-input-multiple-output (MIMO) array has been proposed to reduce the number of elements and channels [8]–[13]. The sparse multi-static linear array proposed by the Pacific Northwest National Laboratory that Tx and Rx arrays separate into two lines does not make full use of the array elements, so the number is still too much [7], [8]. Similarly

The associate editor coordinating the review of this manuscript and approving it for publication was Zhao Zhang.

in the planar multi-static sparse array in which 736 Tx and 736 Rx have been used to achieve an array aperture of around 50 cm × 50 cm, the lateral resolution is about 2.0 mm because the operating frequency band is 72∼80 GHz and the target distance is 0.5 m [9]. Simultaneously, another sparse array named linear sparse periodic antenna array (SPA) have been proposed particularly for the personnel screening systems [10]–[13]. And there are different schemes to achieve 2D scanning when using a linear SPA. One example is to use the rotation of a quasi-optic mirror to scan along the vertical direction in a horizontal linear SPA imaging system with 4 Tx and 16 Rx elements operating at 340 GHz [10], [11]. The anticipated theoretical resolution is 14 mm at a target distance of 3 m, but the images constructed in experiment show the much poorer resolution. This is due to not only a short array length (small aperture) being used, but also the quasi-optical scanning scheme (data sampling method) not receiving reflected signals well when the incident beams have an obvious tilted angle onto the target surface during the scanning. In contrast, the imaging system that scans along the vertical direction by moving mechanically the horizontal linear SPA has achieved better image quality at a short target distance of around 0.5 m when operating in the frequency band of 2.8∼19.5 GHz [12] or 0.6 m when operating in the frequency band of 75∼90 GHz [13], respectively. Thus, we have adopted this kind of imaging scheme with a moving linear SPA operating at the W band in this study as a trade-off between the image resolution and system cost.

The compressive sensing theory has indicated an unknown sparse signal can be exactly recovered with far fewer samples or measurements than traditionally required [14], [15]. It can help to either reduce the cost by adopting fewer channels or increase the frame rate by sampling fewer samples, so this CS technique has been successfully applied to many imaging applications including radar imaging [16], [17], THz imaging [18]–[20], MMW holography [21]–[23], microwave synthetic aperture radar (SAR) imaging [24]–[27], ISAR imaging [28] and MMW phase array imaging [29]. However, the experimental work on the MMW/THz imaging system using CS reconstruction is rather limited since the random sampling in CS theory is complicated to be implemented in practice. The earliest proof-of-concept test of CS MMW imaging was conducted in a single pixel 100 GHz imaging system that uses either a random pattern to partially allow the beam to be transmitted [18] or a raster scan moved along a under sampling pattern [19]. Alternatively, the CS imaging experiments can be carried out by using an under sampling pattern or a random mask matrix consisting of zero and one to choose part of the fully measured data obtained by the raster scanning with one single Tx/Rx pair [20]–[23]. Nevertheless, these studies are based on the monostatic scenario and that the sampling or scanning with single Tx/Rx pair is simple in the experiments. However, the MIMO/SPA is a multi-static scenario where the exact positions of Tx and Rx should be used for a much more complicated image reconstruction. Therefore, we have not only firstly investigated the CS application in the multi-static array imaging scheme and accordingly proposed the discrete SPA-CS model for the image reconstruction, but also devised a simplified experimental system to successfully verify the imaging model.

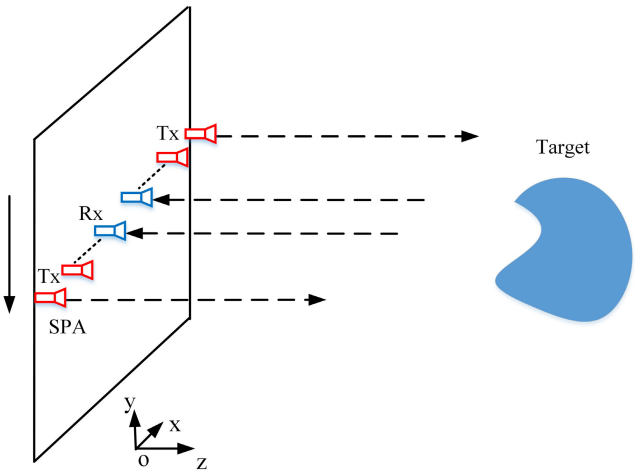


**FIGURE 1.** Imaging scheme with SPA for horizontal scanning.

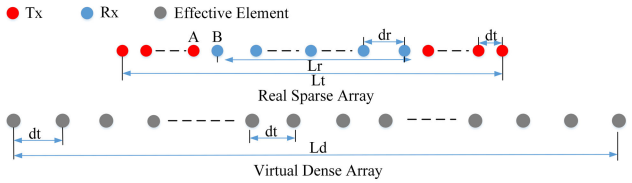


**FIGURE 2.** Sparse periodic antenna array set-up and effective aperture.

The rest of the paper is organized as follows. Section II introduces the proposed W band SPA imaging scheme for the personnel screening and proposes the discrete SPA-CS imaging model for such a multi-static array imaging system. Section III discusses the result reconstructed by the traditional holographic/SAR imaging algorithm based on the simulated and experimental data of imaging a testing target and compares it with the CS reconstruction method using the experimental data. Section IV concludes this work.

## II. PROPOSED W BAND SPA IMAGING SCHEME WITH CS

### A. PROPOSED W BAND IMAGING SCHEME WITH SPA

The scanning scheme used in this paper has been illustrated in Fig. 1. Tx array elements in a linear sparse periodic antenna array are sequentially switched on for electronic scanning along the horizontal direction. After recording the echo data between each Tx-Rx combinations, the array moves to the next vertical sampling point to repeat the previous process until the full 2D aperture data are obtained for the image reconstruction. The SPA properly configured in the scheme [30] can work equivalently to a uniform dense array that has a longer array aperture length $Ld = dt \cdot Nt \cdot Nr$ as shown in Fig. 2, Nt and Nr are the number of transmitting and receiving array elements, so it can achieve a higher resolution with relatively fewer elements.

### B. CS IMAGING WITH THE LINEAR SPA

The compressive sampling process can be described as a matrix form as shown in equation (1). A unknown signal $X_{N\times1}$, if it is not sparse, generally can be represented as a sparse form $SX_{N\times1}$ in another domain by a determined sparse basis function $\Psi_{M\times N}$ that are related to fast Fourier transform(FFT), discrete cosine transform(DCT), discrete wavelet transform (DWT) or more advanced dictionary learning [31], this process is named sparse representation or coding. Then it can be projected onto a low dimension measurement domain by a determined observation matrix $\Phi_{M\times N}$ wherein M is much less than N. If the $\Phi_{M\times N}$ satisfies Restricted Isometry Property (RIP), the unknown $SX_{N\times1}$ can be recovered from a small amount of measurements $Y_{M\times1}$ by a suitable reconstruction algorithm, so then the unknown signal $X_{N\times1}$ can be exactly reconstructed by multiplying a $\Psi^{-1}_{N\times N}$. The RIP can also be interpreted as a simple way that observation matrix $\Phi_{M\times N}$ is incoherent to sparse basis function $\Psi_{M\times N}$.

$$\begin{aligned} Y_{M\times1} &= \Phi_{M\times N}X_{N\times1} \\ &= \Phi_{M\times N}\Psi^{-1}_{N\times N}\Psi_{N\times N}X_{N\times1} \\ &= \Phi_{M\times N}\Psi^{-1}_{N\times N}SX_{N\times1} \\ &= \Theta_{M\times N}SX_{N\times1} \end{aligned} \tag{1}$$

However, the RIP that implies a random sampling process has a challenge in practical application, so this was originally demonstrated by using either plenty of random patters on a planar screen to mimic the random sampling or a mask matrix to select part samples from the full data [18], [19], [22]. Therefore, in order to simplify the verification, we have also used a matrix mask consisting of only 0 and 1 to partly select data from the full S parameters recorded by the SPA. However, this selection could be implemented into the sampling process in the future to further reduce the data acquisition time once the feasibility of the CS reconstruction has been demonstrated and this mask is known.

In this active multi-static SPA imaging system, the echo data/S parameter of *pth* transmitter and *qth* receiver at *wth* mechanical position is the superposition of target reflectivity function *g(x, y, z)* multiplied by the roundtrip phase, calculated as equation (2).

$$s(Tx_{p,w}, Rx_{q,w}) = \iint g(x,y,z)e^{-jk(\left|\vec{R_t}\right|+\left|\vec{R_r}\right|)}dxdy \tag{2}$$

According to equation (2), a discrete version of $s(\mathrm{Tx}_{p,w}, \mathrm{Rx}_{q,w})$ can be represented as equation (3). It is supposed that the target plane reflectivity function *g(x, y, z)* is discretized as a M × N grids and the fully sampled S parameters by the SPA has the NtNr × W sampling positions wherein it is already under-sampled when the NtNrW is less than MN. In order to utilize the standard 1D CS reconstruction algorithm, the discrete multi-static SPA imaging model in equation (3) should be firstly modified by reshaping the 2D S parameters matrix and reflectivity function matrix into long 1D column vectors, as shown in equation (4)

$$s(Tx_{p,w}, Rx_{q,w}) = \sum_{i=1}^{M}\sum_{j=1}^{N} g(i,j)\cdot e^{-jk(\left|\overrightarrow{R_{p,w}^{i,j}}\right|+\left|\overrightarrow{R_{q,w}^{i,j}}\right|)} \tag{3}$$

$$\begin{aligned} S_{Nt\cdot Nr\cdot W\times1} &= \begin{bmatrix} \mathrm{s}(1,1) \\ \vdots \\ s(Nt\cdot Nr,1) \\ \vdots \\ s(1,W) \\ \vdots \\ s(Nt\cdot Nr,W) \end{bmatrix} \\ &= \begin{bmatrix} H(1\cdot1,1) \\ \vdots \\ H(Nt\cdot Nr,1) \\ \vdots \\ H(1\cdot1,W) \\ \vdots \\ H(Nt\cdot Nr,W) \end{bmatrix} \begin{bmatrix} g(1,1) \\ \vdots \\ g(M,1) \\ \vdots \\ g(1,N) \\ \vdots \\ g(M,N) \end{bmatrix} \end{aligned} \tag{4}$$

where

$$\begin{aligned} &H(p\cdot q,w) \\ &= \begin{bmatrix} e^{-jk(\left|\overrightarrow{R_{p,w}^{1,1}}\right|+\left|\overrightarrow{R_{q,w}^{1,1}}\right|)}, & \cdots & e^{-jk(\left|\overrightarrow{R_{p,w}^{M,1}}\right|+\left|\overrightarrow{R_{q,w}^{M,1}}\right|)}, \\ \cdots & e^{-jk(\left|\overrightarrow{R_{p,w}^{1,N}}\right|+\left|\overrightarrow{R_{q,w}^{1,N}}\right|)}, & \cdots & e^{-jk(\left|\overrightarrow{R_{p,w}^{M,N}}\right|+\left|\overrightarrow{R_{q,w}^{M,N}}\right|)} \end{bmatrix} \end{aligned} \tag{5}$$

Afterwards, in order to solve the CS equations, the discrete multi-static SPA-CS imaging model as general matrix form in equation (1) could be derived as illustrated in equation (6).

$$\begin{aligned} y_{V\times1} &= A.*S_{NtNrW\times1} \\ &= A.*(H_{NtNrW\times MN}g_{MN\times1}) \\ &= [A.*(H_{NtNrW\times MN}\Psi^{1}_{MN\times MN})]_{V\times MN} \\ &\quad\times(\Psi_{MN\times MN}g_{MN\times1}) \\ &= \Theta_{V\times MN}Sg_{MN\times1} \end{aligned} \tag{6}$$

where $\cdot*$ represents element-wise multiplication. Binary mask **A** is a sampling matrix that only contains 1 (sampled) and 0 (ignored), which makes each row of matrix **H** active or inactive, so ***y*** is a vector sampling the number of V of the S parameters recorded by this SPA imaging system. When V is less than NtNrW, the sampling data has been further reduced.

Regarding the reconstruction algorithm, they are usually categorized into the convex optimization algorithms such as basis pursuit (BP) and the greedy algorithms like orthogonal matching pursuit (OMP) [14], [32]. As for the large matrixes in this paper that demand for plenty of computer resource, we have obtained the reconstruction result through the SPGL1 algorithm that suits for the large-scale sparse reconstruction [32]. What we have used is to minimize the

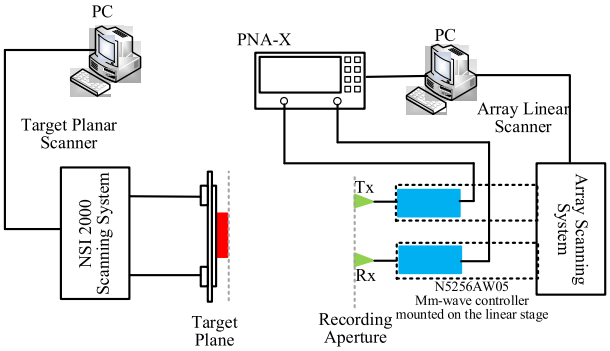


**FIGURE 3.** Schematic of the SPA experimental imaging system.

$l_1$ norm of the sparse form of target reflectivity function subjected to the condition as shown in equation (7) where the $\sigma$ is the tolerance between the solution and measured data.

$$\text{minimize } \|Sg\|_1 \quad \text{subject to } \|\Theta Sg - y\|_2 < \sigma \qquad (7)$$

## III. SIMULATION STUDY AND THE PROOF OF CONCEPT TEST

In order to verify the proposed imaging scheme experimentally, thus, we have conducted the proof-of-concept experiments with a simplified 94 GHz imaging system using 1 Tx and 1 Rx whose schematic is shown in Fig. 3. Consequently, the whole set-up in the lab is photographed in Fig. 4(a). In order to realize the linear SPA, two THz mixer heads highlighted in blue in the Fig. 3 are mounted on two linear horizontal scanning stages separated by a gap as shown in Fig. 4(b), moving to each Tx and Rx element positions in the SPA. In addition, the testing target is mounted on the NSI 2000 scanning head, moving vertically, as shown in Fig. 4(c), which inversely imitates a relatively mechanical scanning of the array to a fixed target. In order to simplify the study, the testing target in this preliminary stage is a rectangular metal plate ($145\times120\times5\text{mm}^3$) without any dielectric, having a number of holes (diameters of 6 cylinder holes are 6 mm and 7 mm; top and bottom diameters of 4 screw holes are 5 mm and 8 mm). It is worth to mention that the effect of the vertical gap between Tx and Rx elements is found not to be significant, but it is still desired to keep it as small as possible to guarantee its performance) [33]. Therefore, the minimum gap of 192 mm for the smooth scanning movement of Tx and Rx mixers heads has been chosen. This experimental setup only uses one Tx and one Rx channel to imitate Tx and Rx arrays, respectively. This approach not only avoids using a large number of real channels in high cost, but also eliminates the phase calibration issue in the experiment.

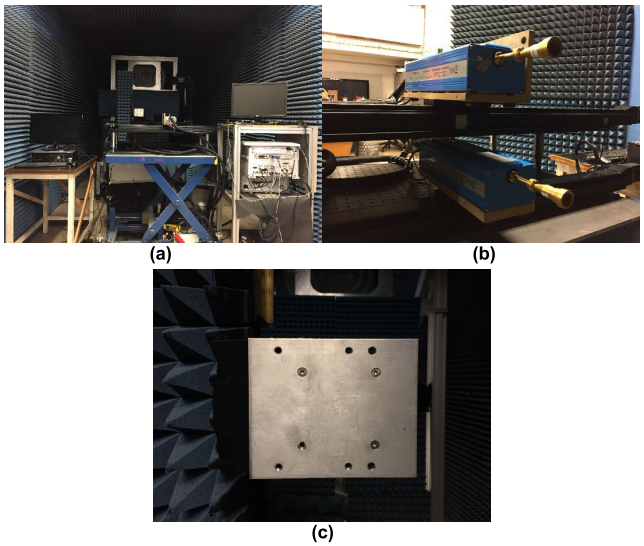


**FIGURE 4.** Photographs of the experimental set-up (a) whole view of the system, (b) closer view of the horizontal linear scanning stages and (c) the testing target: a rectangular metal plate ($145\times120\times5$ mm$^3$) with 10 holes.

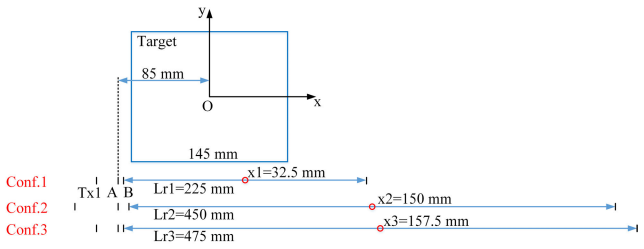


**FIGURE 5.** Positions of three configurations in simulation.

**TABLE 1.** Practical resolutions calculated by equation (8) (units: mm).

| Config. | Tx & Rx | Lt | $\theta_b$ | HPBW | Practical Resolutions at (1.3 m) |
|---|---|---|---|---|---|
| 1 (dt=5) | 10 & 10 | 275 | 12.075 | 13° | 7.586 mm |
| 2(dt=10) | 10 & 10 | 550 | 23.888 | 13° | 7.048 mm |
| 3(dt=5) | 10 & 20 | 525 | 22.832 | 13° | 7.048 mm |

### A. COMPARISON OF IMAGING IN SIMULATION AND EXPERIMENT

Firstly, we have investigated the image reconstruction using the traditional holographic/SAR imaging algorithm on three configurations as illustrated in Fig. 5 and the parameters are listed in TABLE 1. Both configurations 1 and 2 have 10 Tx elements and 10 Rx elements, but with different Tx element spacing, so the effective length of configuration 2 is twice as long as configuration 1. In contrast, we keep the Tx element spacing in configuration 1 and 3 same but double the number of Rx elements in configuration 3, so the effective length is doubled as well, same as configuration 2. Besides, we made the last left-side Tx element denoted by letter **A** as a reference whose positions in three configurations are same. Meanwhile, the target has been placed slightly to the left side, closing to the referenced Tx element to assure a good illumination and the corrugated horns utilized in the experiments have a measured peak gain of about 17.19 dB and a HPBW at H plane of about 13°. Therefore, the practical resolution taking account of this narrow beam-width can be calculated

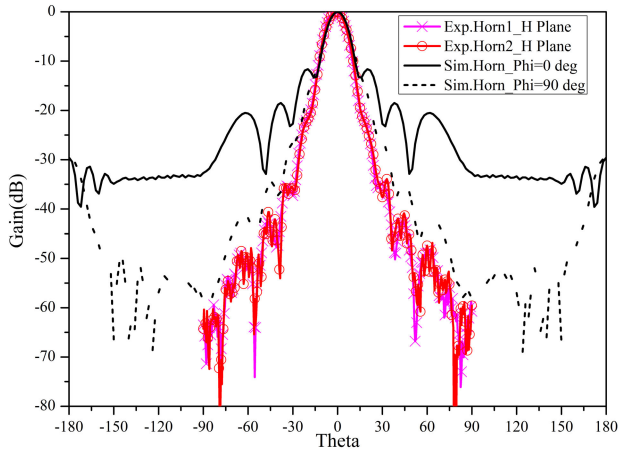


**FIGURE 6.** Comparison between the measured H plane pattern of the horns used in the experiments and the simulated pattern in the configurations study ($f = 94$ GHz).

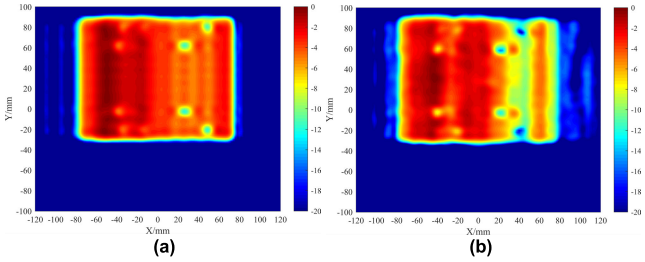


**FIGURE 7.** Reconstructed images of the configuration 1 in Table 1: (a) simulated and (b) measured.

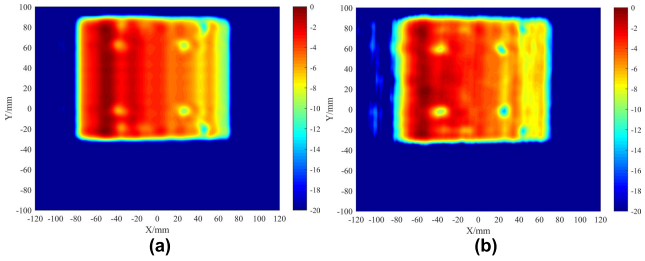


**FIGURE 8.** Reconstructed images of the configuration 2 in Table 1: (a) simulated and (b) measured.

by equation (8) [22], [33], as shown in TABLE 1.

$$\Delta = \lambda \big/ (4 \cdot \sin(\theta \big/ 2))|_{\theta = \min(\theta_{HPBW}, \theta_b)} \tag{8}$$

wherein $\theta_b = 2\tan^{-1}(Lt/(2D))$ is the angle subtended by the scanning aperture.

Consequently, the simulations were conducted in the commercial software of FEKO$^{TM}$ by using a horn with a similar HPBW at H plane in comparison with the experiments. So the simulated pattern of the horns used in the imaging simulation and the measured H plane pattern of the horns used in the experiments are shown in Fig. 6 in which the operation frequency is 94 GHz. The images based on the simulated and measured data have been compared in (a) and (b) of Fig. 7, Fig. 8 and Fig. 9, respectively. As shown in the simulated results, three configurations have shown similar resolutions

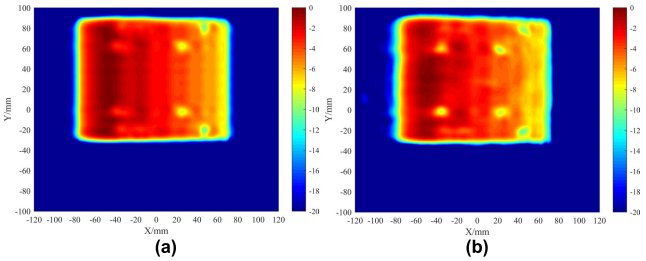


**FIGURE 9.** Reconstructed images of the configuration 3 in Table 1: (a) simulated and (b) measured.

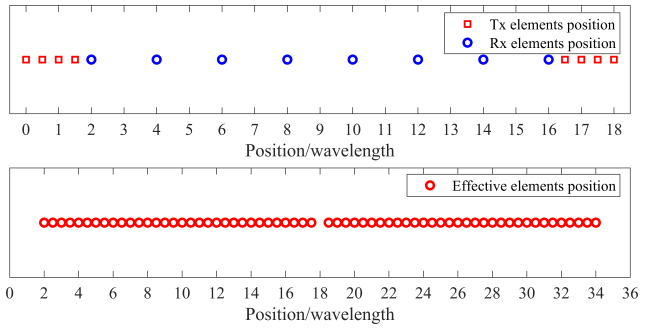


**FIGURE 10.** Illustration of the SPA with 8 Tx & 8 Rx and its 64 sampling points.

of around 7.0 mm, as indicated in TABLE 1. It indicates that the resolution is improving toward to the array centre since the phase shift between sampling points is decreasing while the image quality is deteriorating (here, this means to increasing contrast) since the illumination from the Tx elements placed at two ends is becoming weaker. Therefore, the reconstructed image of configuration 1 has shown the best resolution and image quality since its target is close to both the Tx elements and array centre due to its compact array size. In addition, the resolutions in configuration 2 and 3 deteriorate little since the target is far away from the array centre and the contrast at right edge of the target is worse since the illumination from Tx elements becomes weaker. In contrast, the experimental images have already shown the consistent resolutions with the simulated results except the image quality (contrast) in a small part of image of configuration 1 deteriorates little. That is because, in addition to the difference in illumination power at the centre and two ends of the target, the sampling by this SPA technique has one central sampling point missed, as one example of 8 Tx and 8 Rx illustrated in Fig. 10. This effect has already been indicated in the simulated image of configuration 1 where the centre position of the array corresponds to the axis $x = 32.5$ mm in the image. Furthermore, it has also been verified by the simulated and measured results in our study on a 220 GHz imaging that this issue will become more obvious when the beam width is relatively narrow to the target distance or element spacing [33]. As shown in Fig. 6, the pattern (out of HPBW) of the horns used in the experiments is already little bit narrower than the ones in simulation. In addition, the practical sensitivity of the imaging system is not as ideal as the

**TABLE 2.** Comparison between the other research and my work.

| Ref. | $f$ (BW) | dt(mm) | Tx/Rx | D(m) | $\delta_T$ | $\delta_E$ |
|---|---|---|---|---|---|---|
| [11] | 340G(16G) | $2(3.4\lambda_c)$ | 4/16 | 3.0 | 14 | Low |
| [13] | 75~90 G | $2(0.55\lambda_c)$ | 16/26 | 0.6 | 2.26 | 2.3 |
| Ours (2) | 94 G | $10(3.12\lambda_c)$ | 10/10 | 1.3 | 7.05 | 7.0 |

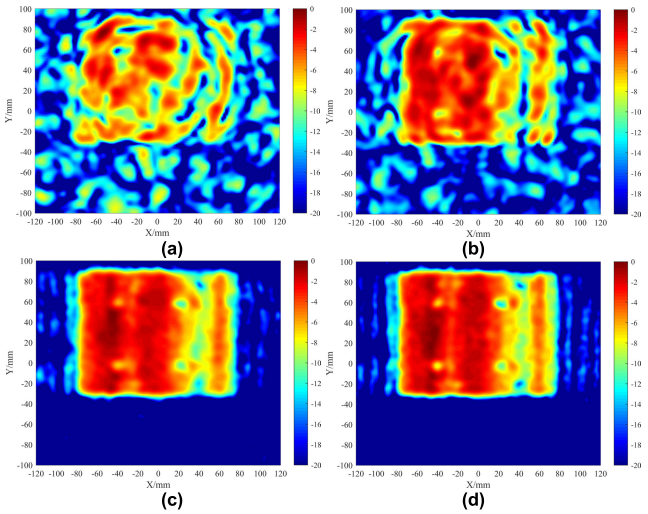


**FIGURE 11.** Reconstructed images of the configuration 1 by the traditional holographic/SAR approach with (a) 20% (b) 40% experimental data and the proposed CS approach with (c) 20% (d) 40% experimental data.

simulated one, which is equivalent to further reducing the beam width. Fortunately, this issue can be solved by reducing the element spacing, using wider beam-width or increasing the target distance.

In order to demonstrate the effectiveness of our proposed imaging system, we have made a comparison between our work and 2 representative SPA work in TABLE 2, in terms of image resolution $\delta_T$ (theoretical) and $\delta_E$ (experimental). It is shown that although operating at a sub-millimetre wave frequency of 340 GHz in [10], [11], the image resolution is worse than 14 mm at a target distance of 3 m in experiment because of the deployment of fewer expensive Tx elements (4) and quasi-optical rotating scanning scheme and a long target distance. The SPA imaging system in the band of 75~90 GHz in [13] has shown a brilliant image resolution of 2.26 mm in the experiment with a target at 0.6 m due to the utilisation of larger number of cheap Tx/Rx elements(40) and short target distance. The measured resolution in our proposed imaging system at W band based on configuration 2 in Table 1 is around 7 mm, which is below the stringent limit (10 mm) for personnel screening [34]. Though the resolution is lower than that of [13], it is fair to say that our proposed SPA imaging system has reached a good balance between image quality and system cost since only half of the Tx/Rx elements were deployed and the target distance is more than doubled.

### B. EXPERIMENTAL IMAGES USING CS RECONSTRUCTION

Next, we have investigated the CS reconstruction based on the experimental data of the configurations 1 and 3. This

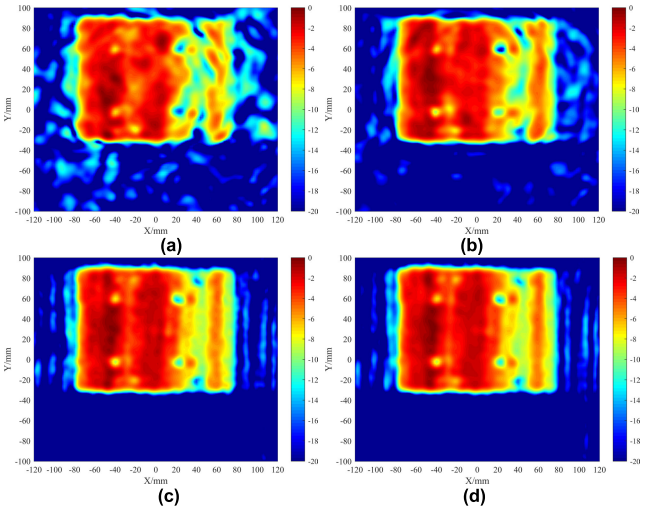


**FIGURE 12.** Reconstructed images of the configuration 1 by the traditional holographic/SAR approach with (a) 60% (b) 80% experimental data and the proposed CS approach with (c) 60% (d) 80% experimental data.

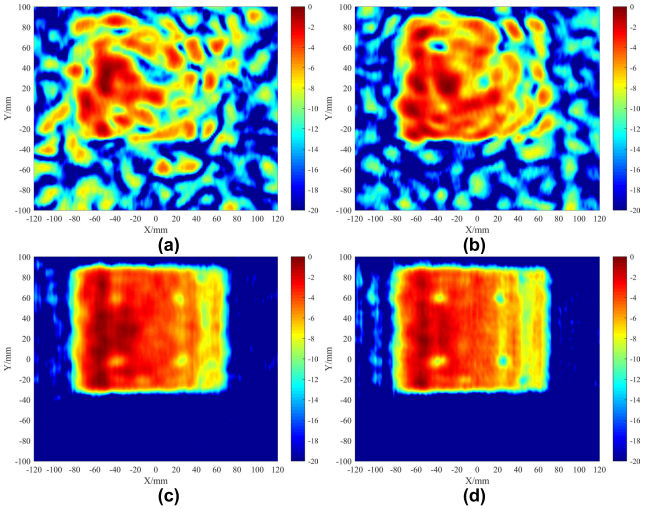


**FIGURE 13.** Reconstructed images of the configuration 2 by the traditional holographic/SAR approach with (a) 20% (b) 40% experimental data and the proposed CS approach with (c) 20% (d) 40% experimental data.

has been demonstrated in the simulation study that CS can alleviate the aliasing and also reconstruct image successfully with much less data [35]. Therefore, the experimental images of the configuration 1 reconstructed by the traditional holographic/SAR approach and the proposed CS approach with 20%, 40% and 60%, 80% sampling data are shown in Fig. 11 and Fig. 12, respectively. Similarly, the experimental images of the configuration 2 and 3 are shown in Fig. 13, Fig. 14 and Fig. 15, Fig. 16, respectively. It is shown that the traditional holographic/SAR approach is not capable of reconstructing the target properly when the data randomly redundancy is large (>20%). On the contrary, the proposed CS approach is capable of achieving the image reconstruction even when the data randomly redundancy is as large as 80%. The proposed CS approach is capable of reconstructing

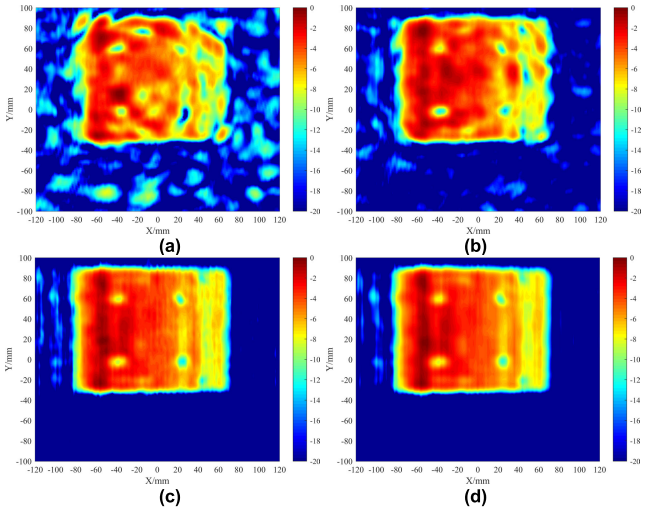


**FIGURE 14.** Reconstructed images of the configuration 2 by the traditional holographic/SAR approach with (a) 60% (b) 80% experimental data and the proposed CS approach with (c) 60% (d) 80% experimental data.

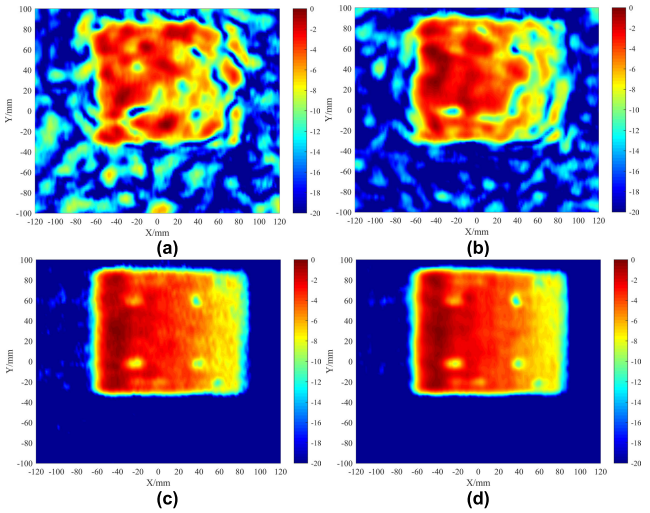


**FIGURE 15.** Reconstructed images of the configuration 3 by the traditional holographic/SAR approach with (a) 20% (b)40% experimental data and the proposed CS approach with (c) 20% (d) 40% experimental data.

a good quality image with only 40% sampling data, compared to 100% data using the traditional holographic/SAR approach.

Finally, we have assessed the effect of signal noise on this CS reconstruction scheme using the simulated data in configuration 1 with the added Gaussian noise of 3 different grades of signal to noise ratio (SNR): 5 dB, 10 dB and15 dB, respectively. The images are constructed based on 80% of the data chosen randomly and compared in Fig. 17. It is shown that the obvious speckles will appear when the SNR is lower than 10 dB, leading to the degradation of the image quality. When the SNR being increased to 15 dB, the noise almost has no effect on the constructed image. Therefore, we have always kept the SNR higher than 15 dB in the Rx channel in the experiment.

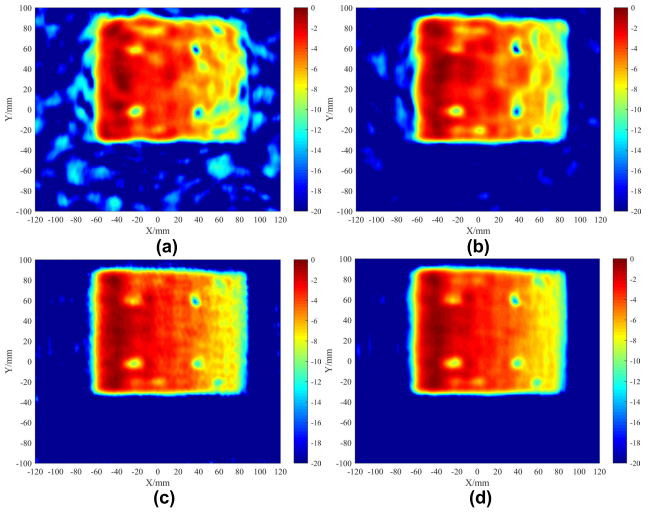


**FIGURE 16.** Reconstructed images of the configuration 3 by the traditional holographic/SAR approach with (a) 60% (b)80% experimental data and the proposed CS approach with (c) 60% (d) 80% experimental data.

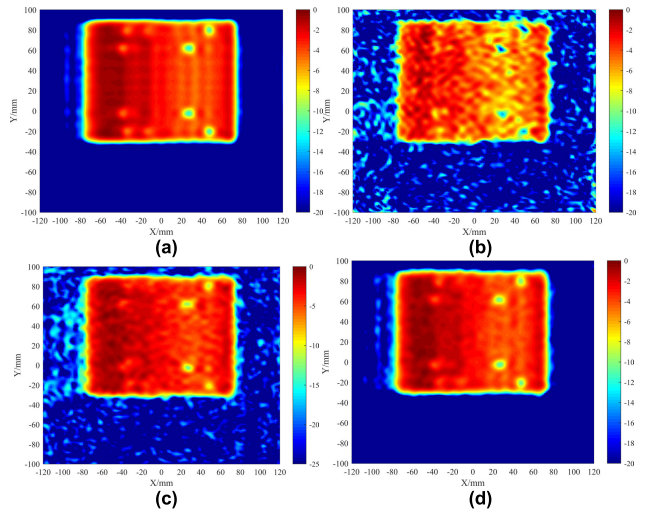


**FIGURE 17.** The reconstructed images by the proposed CS approach with 80% of the simulated data of the configuration 1. (a) No added noise, and added Gaussian noise in (b) 5 dB SNR, (c) 10 dB SNR and (d) 15 dB SNR.

## IV. CONCLUSIONS

This paper presents our study on the CS imaging scheme with a combination of mechanical and electronic scanning achieved by a linear SPA operating at W band. Meanwhile, a simplified experimental THz imaging system with only 1 Tx and 1 Rx channels has been used successfully in the proof-of-concept demonstration. Consequently, the experimental results have shown an excellent consistency with the simulated ones. The CS reconstruction is capable of dramatically reducing the sampling points while maintaining a good image quality, leading to a decrease of data acquisition time in the practical application.

## REFERENCES

[1] M. Kowalski, M. Kastek, M. Walczakowski, N. Palka, M. Szustakowski, "Passive imaging of concealed objects in terahertz and long-wavelength infrared," *Appl. Opt.*, vol. 54, no. 13, pp. 3826–3833, May 2015.
[2] M. Kowalski and M. Kastek, "Comparative studies of passive imaging in terahertz and mid-wavelength infrared ranges for object detection," *IEEE Trans. Inf. Forensics Security*, vol. 11, no. 9, pp. 2028–2035, Sep. 2016.
[3] E. Heinz, T. May, D. Born, G. Zieger, S. Anders, V. Zakosarenko, H.-G. Meyer, and C. Schäffel "Passive 350 GHz video imaging systems for security applications," *J. Infr., Millim., THz. Waves*, vol. 36, no. 10, pp. 879–895, Oct. 2015.
[4] E. Heinz, *Toward High-Sensitivity and High-Resolution Submillimeter-Wave Video Imaging*. Bellingham, WA, USA: SPIE, 2011, p. 9.
[5] S. Rowe, E. Pascale, S. Doyle, C. Dunscombe, P. Hargrave, A. Papageorgio, K. Wood, P. A. R. Ade, P. Barry, A. Bideaud, T. Brien, C. Dodd, W. Grainger, J. House, P. Mauskopf, P. Moseley, L. Spencer, R. Sudiwala, C. Tucker, and I. Walker, "A passive terahertz video camera based on lumped element kinetic inductance detectors," *Rev. Sci. Instrum.*, vol. 87, no. 3, Mar. 2016, Art. no. 033105.
[6] R. Appleby and H. B. Wallace, "Standoff detection of weapons and contraband in the 100 GHz to 1 THz region," *IEEE Trans. Antennas Propag.*, vol. 55, no. 11, pp. 2944–2956, Nov. 2007.
[7] D. Sheen, D. McMakin, and T. Hall, "Near-field three-dimensional radar imaging techniques and applications," *Appl. Opt.*, vol. 49, no. 19, pp. E83–E93, 2010.
[8] D. M. Sheen and T. E. Hall, "Reconstruction techniques for sparse multistatic linear array microwave imaging," *Proc. SPIE*, vol. 9078, Jun. 2014, Art. no. 90780I.
[9] S. S. Ahmed, A. Schiessl, and L.-P. Schmidt, "A novel fully electronic active real-time imager based on a planar multistatic sparse array," *IEEE Trans. Microw. Theory Techn.*, vol. 59, no. 12, pp. 3567–3576, Dec. 2011.
[10] J. Gao, Z. Cui, B. Cheng, Y. Qin, X. Deng, B. Deng, X. Li, and H. Wang, "Fast three-dimensional image reconstruction of a standoff screening system in the terahertz regime," *IEEE Trans. THz Sci. Technol.*, vol. 8, no. 1, pp. 38–51, Jan. 2018.
[11] B. Cheng, Z. Cui, B. Lu, Y. Qin, Q. Liu, P. Chen, Y. He, J. Jiang, X. He, X. Deng, J. Zhang, and L. Zhu, "340-GHz 3-D imaging radar with 4Tx-16Rx MIMO array," *IEEE Trans. THz Sci. Technol.*, vol. 8, no. 5, pp. 509–519, Jul. 2018.
[12] X. Zhuge and A. G. Yarovoy, "A sparse aperture MIMO-SAR-based UWB imaging system for concealed weapon detection," *IEEE Trans. Geosci. Remote Sens.*, vol. 49, no. 1, pp. 509–518, Jan. 2011.
[13] F. Gumbmann and L. Schmidt, "Millimeter-wave imaging with optimized sparse periodic array for short-range applications," *IEEE Trans. Geosci. Remote Sens.*, vol. 49, no. 10, pp. 3629–3638, Oct. 2011.
[14] D. L. Donoho, "Compressed sensing," *IEEE Trans. Inf. Theory*, vol. 52, no. 4, pp. 1289–1306, Apr. 2006.
[15] A. Massa, P. Rocca, and G. Oliveri, "Compressive sensing in electromagnetics—A review," *IEEE Antennas Propag. Mag.*, vol. 57, no. 1, pp. 224–238, Feb. 2015.
[16] A. B. Suksmono, E. Bharata, A. A. Lestari, A. G. Yarovoy, and L. P. Ligthart, "Compressive stepped-frequency continuous-wave ground-penetrating radar," *IEEE Geosci. Remote Sens. Lett.*, vol. 7, no. 4, pp. 665–669, Oct. 2010.
[17] V. M. Patel, G. R. Easley, D. M. Healy, Jr., and R. Chellappa, "Compressed synthetic aperture radar," *IEEE J. Sel. Topics Signal Process.*, vol. 4, no. 2, pp. 244–254, Apr. 2010.
[18] W. L. Chan, K. Charan, D. Takhar, K. F. Kelly, R. G. Baraniuk, and D. M. Mittleman, "A single-pixel terahertz imaging system based on compressed sensing," *Appl. Phys. Lett.*, vol. 93, no. 12, pp. 121105-1–121105-3, Sep. 2008.
[19] W. L. Chan, M. L. Moravec, R. G. Baraniuk, and D. M. Mittleman, "Terahertz imaging with compressed sensing and phase retrieval," *Opt. Lett.*, vol. 33, no. 9, pp. 974–976, 2008.
[20] V. M. Patel and J. N. Mait, "Compressive passive millimeter wave imaging with extended depth of field," *Proc. SPIE*, vol. 51, no. 9, Jun. 2012, Art. no. 091610.
[21] C. F. Cull, D. A. Wikner, J. N. Mait, M. Mattheiss, and D. J. Brady, "Millimeter-wave compressive holography," *Appl. Opt.*, vol. 49, no. 19, pp. E67–E82, 2010.
[22] Q. Cheng, A. Alomainy, and Y. Hao, "On the performance of compressed sensing-based methods for millimeter-wave holographic imaging," *Appl. Opt.*, vol. 55, no. 4, pp. 728–738, 2016.
[23] L. Qiao, Y. Wang, Z. Shen, Z. Zhao, and Z. Chen, "Compressive sensing for direct millimeter-wave holographic imaging," *Appl. Opt.*, vol. 54, no. 11, pp. 3280–3289, 2015.
[24] J. Yang, J. Thompson, X. Huang, T. Jin, and Z. Zhou, "Random-frequency SAR imaging based on compressed sensing," *IEEE Trans. Geosci. Remote Sens.*, vol. 51, no. 2, pp. 983–994, Feb. 2013.
[25] H. Kajbaf, J. T. Case, Z. Yang, and Y. R. Zheng, "Compressed sensing for SAR-based wideband three-dimensional microwave imaging system using non-uniform fast Fourier transform," *Radar, Sonar Navigat., IET*, vol. 7, no. 6, pp. 658–670, Jul. 2013.
[26] J.-C. Ni, Q. Zhang, Y. Luo, and L. Sun, "Compressed sensing SAR imaging based on centralized sparse representation," *IEEE Sensors J.*, vol. 18, no. 12, pp. 4920–4932, Jun. 2018.
[27] W. Qiu, J. Zhou, H. Zhao, and Q. Fu, "Three-dimensional sparse turntable microwave imaging based on compressive sensing," *IEEE Geosci. Remote Sens. Lett.*, vol. 12, no. 4, pp. 826–830, Apr. 2015.
[28] X. Pan, J. Liu, J. Chen, Q. Xie, and X. Ai, "Sub-Nyquist sampling jamming against chirp-ISAR with CS-D range compression," *IEEE Sensors J.*, vol. 18, no. 3, pp. 1140–1149, Feb. 2018.
[29] Q. Cheng, A. Alomainy, and Y. Hao, "Compressive millimeter-wave phased array imaging," *IEEE Access*, vol. 4, pp. 9580–9588, 2016.
[30] G. R. Lockwood, P. C. Li, M. O'Donnell, and F. S. Foster, "Optimizing the radiation pattern of sparse periodic linear arrays," *IEEE Trans. Ultrason., Ferroelectr., Freq. Control*, vol. 43, no. 1, pp. 7–14, Jan. 1996.
[31] Z. Zhang, W. Jiang, J. Qin, L. Zhang, F. Li, M. Zhang, and S. Yan, "Jointly learning structured analysis discriminative dictionary and analysis multiclass classifier," *IEEE Trans. Neural Netw. Learn. Syst.*, vol. 29, no. 8, pp. 3798–3814, Aug. 2018.
[32] E. van de Berg and M. P. Friedlander. (2007). *SPGL1: A Solver for Large-Scale Sparse Reconstruction*. [Online]. Available: Available: https://www.cs.ubc.ca/~mpf/spgl1/
[33] S. Hu, C. Shu, Y. Alfadhl, and X. Chen, "A THz imaging system using linear sparse periodic array," *IEEE Sensors J.*, to be published.
[34] M. C. Kemp, "Millimetre wave and terahertz technology for the detection of concealed threats—A review," *Proc. SPIE*, vol. 6402, pp. 647–648, Oct. 2008.
[35] S. Hu, X. Chen, and Y. Alfadhl, "Study on 94GHz imaging system using sparse periodic linear antenna array and compressive sensing," in *Proc. 11th UK-Europe-China Workshop Millimetre Waves THz. Technol. (UCMMT)*, Sep. 2018.

**SHAOQING HU** received the B.S. and M.S. degrees in electronic engineering from the University of Electronic Science and Technology of China, in 2013 and 2016, respectively. He is currently pursuing the Ph.D. degree with the Queen Mary University of London. He has been with the Queen Mary University of London, since 2016. His research interests include wideband circularly polarized antennas, sparse antenna arrays, millimetre wave, and THz imaging for personnel screening. He has already published many articles in these fields and obtained Student Paper Award in 2015 Asia-Pacific Conference on Antennas and Propagation. In addition, he also serves as a Reviewer for many international conferences and journals, such as IEEE Access, and the *Microwave and Optical Technology Letters*.

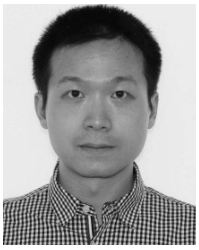

**CHAO SHU** received the B.S. and M.S. degrees in communication and information system from the Beijing University of Posts and Telecommunication, in 2005 and 2008, respectively. He is currently pursuing the Ph.D. degree with the Queen Mary University of London. From 2008 to 2016, he was with Datang Mobile Communications Equipment Company, Ltd., as a Software Engineer and then as the Division Manager. He has been with the Queen Mary University of London, since 2016. He has authored a number of articles on these topics, and he holds 11 granted and pending CN patents. His research interests include wideband circularly polarized antennas, millimetre wave, and THz communication and imaging systems.

**YASIR ALFADHL** was born in Najaf, Iraq, in 1978. He received the B.S. degree in telecommunication engineering from the Queen Mary University of London, London, U.K., in 2000, and the Ph.D. degree in electromagnetics and antennas in telecommunication engineering from the University of London, London, in 2006. He has started a postdoctoral project, where he designed and prototyped a novel base-station antenna for semi-smart cellular networks, as a part of a consultancy project for the Office of Communication-regulatory authority body for the U.K. communications industries. He was a Knowledge Transfer Associate and the Manger of the industry, where he developed 3-D modeling methods for radar and telecom applications. Since 2009, he has served as a Faculty Member of the School of Electronic Engineering and Computer Science, Queen Mary University of London, as a joint-Program Lecturer. Since 2006, he has authored or coauthored over 30 publications. His current research interests include computational electromagnetics, high-power microwave devices, bio-electromagnetics, and dielectric properties of materials. He was a member of the Organizing Committee at the IEEE International Workshop on Antenna Technology: Small and Smart Antennas Conference in Cambridge, in 2007. He was nominated (one of the top 20 in the U.K.) by the Institute of Directors for the KTP Business Leader of Tomorrow Awards in 2009.

**XIAODONG CHEN** (M'96–SM'07–F'14) received the B.Sc. degree in electronics engineering from the University of Zhejiang, Hangzhou, China, in 1983, and the Ph.D. degree in microwave electronics from the University of Electronic Science and Technology of China, Chengdu, China, in 1988. He joined the Department of Electronic Engineering, King's College, University of London, London, U.K., in 1988, as a Post-Doctoral Visiting Fellow. In 1990, he was employed by King's College as a Research Associate, and was appointed to an EEV Lectureship later on. In 1999, he joined the School of Electronic Engineering and Computer Science, Queen Mary University of London, London, where he is currently a Professor with the School of Electronic Engineering and Computer Science. He is also the Director of the BUPT-QMUL Joint Research Lab, Beijing. He holds Visiting Professorships at the University of Westminster, U.K., Beijing University of Posts and Telecommunications (BUPT), and the University of Electronic Science and Technology of China. He has authored or coauthored over 400 publications (book chapters, journal papers, and refereed conference presentations). His current research interests include high-power microwave devices, wireless communications, and antennas. He is also a member of the U.K. Engineering and Physical Sciences Research Council Review College and the Technical Panel of the Institution of Engineering and Technology Antennas and Propagation Professional Network. He is a Fellow of the IET.